FACULTY OF SCIENCE
UNIVERSITY OF COPENHAGEN

Localization of hepatitis B vaccine in SBA-15: A new method of delivery

Bachelor thesis by:
Martin Kjærulf Rasmussen
jfm802@alumni.ku.dk

Supervisor:
Heloisa N. Bordallo
Niels Bohr Institute
University of Copenhagen

Submitted: Wednesday 10th June, 2015

Abstract

SBA-15's porous structure and non-toxicity is promising as an adjuvant for many new oral vaccines, as the porous structure can protect the vaccines from the gastric acid, including Hepatits B vaccine. However, the main component in Hepatitis B vaccine, the HBsAg protein, is too large to fit in the micro and mesopores of SBA-15, which have diameters less than 2 nm and 10 nm respectively. Therefore it is not clear how the vaccine is distributed in the SBA-15 structure.

In this work, thermal analysis, FTIR and imaging using X-ray and neutrons were used to localise the HBsAg protein within the SBA-15 structure. Thermal analysis and FTIR showed that HBsAg can be confined in two ways in SBA-15, while from the imaging results it could be concluded that confined HBsAg agglomerates in branching structures inside the grains of the SBA-15 powder. From the structural analysis it was observed that these agglomerations are anchored by HBsAg in the largest pores in the SBA-15 structure i.e the macropores which are larger than 50 nm. The agglomerated HBsAg was shown to not necessarily distribute uniformly throughout the SBA-15.

Contents

Acknowledgements

I wish to thank my supervisor Heloisa Bordallo, for always having an open office, answering all of my questions, providing guidance and showing great interest throughout the entire project. I also want to thank Márcia Fantini at the University of São Paulo, for providing samples, discussing my results and helping me to understand the SBA-15 structure.
Additional I wish to thank Nikolay Kardjilov for doing the neutron and X-ray imaging at the Helmholtz Center Berlin, and showing me how to data analysis the images. Torsten Lauridsen(NBI) and Carsten Gundlach(DTU) also have my gratitude for helping me do X-ray images at DTU's Imaging Portal. I also thank Markus Strobl and Murillo Longo for coming with inputs and proof reading. Lastly I thank Danscatt for funding my travel to the Helmholtz Center, Berlin.

1 Introduction

Hepatitis B is a disease which attacks the liver. The World Health Organization(WHO) estimates that 2 billion people have been infected with Hepatitis B virus and that 240-400 millions are chronically infected[1]. It is estimated that every year, 130,000 people die from accute Hepatits B infection, and 650,000 people die of sequelae caused by chronic infection[2]. The highest exposure to Hepatitis B occurs in sub-Sharan Africa, where 5-10% of the population is chronically infected. Other high exposed regions are East Asia, the Amazon region and south eastern Europe. Acute hepatitis B has no treatment, as only the related symptoms can be treated. Medical drugs can often stall the replication of virus, but rarely cures chronic infection. The best way to stop hepatitis B is by prevention. The most efficient way to prevent hepatitis B, is by vaccination of infants, as infected infants have 90% risk of developing chronic infection. In countries where efficient vaccination programs have been incorporated, the rate of chronic infection has dropped to below 1%[3].

Vaccination is done by injections of the Hepatitis B surface Antigen(HBsAg) with an adjuvant. The adjuvant is used to increase the immune response, and thereby maximize the efficiency of the vaccine. The most used adjuvant for vaccination of humans is aluminium salt $Al(OH_3)$ (alum), which has been used for 70 years. Alum is generally considered safe for humans, but has some side-effects such as, local irritation, pain, swelling at the injection site, erythema and abscess[4]. Therefore the search for new types of adjuvants, with less side-effects and improved immunological response is an expanding field of research.

SBA-15, a nano structured porous silica can induce an effective immunological response as adjuvant, as good or better than the often used alum salt $Al(OH)_3$[5]. SBA-15 has also been shown to protect the vaccine from the gastric acid, making oral delivery of the vaccine possible[6]. Oral delivery offers significant benefits over injection, such as less side-effect, and better immunological response[7]. Encapsulation of the vaccine within the SBA-15 structure, also makes it possible to store the vaccine at room temperature. This offers a great advantage over other Hepatitis B vaccines, which must be stored at 4°C, when transporting vaccine to areas with bad infrastructure.

The HBsAg protein which is used in Hepatitis B vaccine is too large to fit within the less than 2 nm micropores and 10 nm mesopores in the SBA-15 structure, but SBA-15 has been shown to be able to protect HBsAg from the gastric acids[8]. This raises an interesting question: how does SBA-15 protect HBsAg, and where is HBsAg located within the SBA-15 structure?.

This project aims to localize and describe the distribution of HBsAg within the SBA-15 porous structure. To achieve this aim thermal analysis, including differential scanning calorimetry(DSC), thermogravimetric analysis(TGA) coupled to Fourier transformed infrared spectroscopy(FTIR), X-ray and neutron imaging were used.
The work is presented as follows. In chapters 2 and 3, SBA-15 and the HBsAg protein are described, followed by the presentation of the experimental techniques. In chapter 4 details of the samples and experimental set-ups are given and the results are discussed in chapter 5. The conclusion and perspective of this work are given in chapter 6.

2 Description of SBA-15 and HBsAg

2.1 The structure of SBA-15

Santa Barbara Amorphous(SBA-15) named after the university at which it was discovered, University of California, Santa Barbara, has a porous structure on three different length scales, macropores, hexagonal ordered mesopores and micropores. The size of these pores can be manipulated during the synthesis of SBA-15[9]. In this project the samples used have mesopores with a mean diameter of 10 nm and micropores with diameter less than 2 nm. The mesopores are ordered hexagonally in regions of about 300 nm in diameter, where the mesopores are orientated in the same direction. These regions are neighbours to other regions where the hexagonal ordered mesopores are orientated differently, as can be seen in fig.1(A). The micropores are small channels that connect the ordered mesopores through the mesopore walls.
The regions of ordered mesopores form larger rod like structures with a length of about 2 microns, as seen in fig.1(B). The orientation of these rods are random, and the empty voids between the rods are the macropores with a diameter larger than 50 nm.

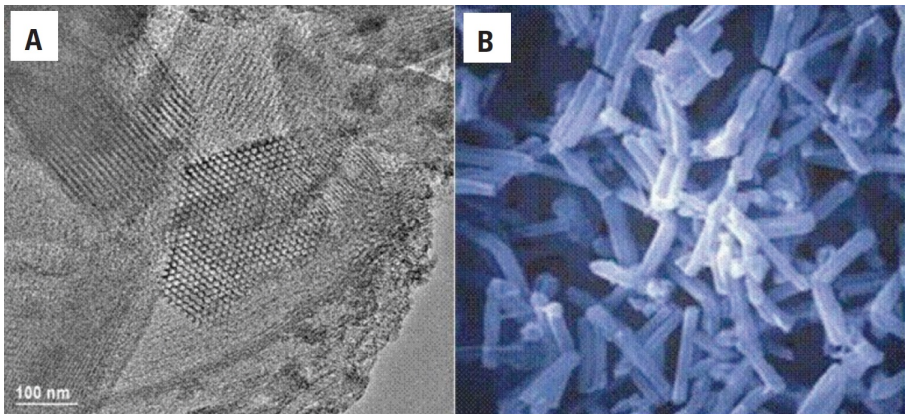

Figure 1: (A) Transmission electron microscopy image of the hexagonal ordered mesopores with a mean diameter of 10 nm. (B) Scanning electron microscopy image of the SBA-15 rods with mean length 2 μm, the voids between the rods is the macropores. Reprint from (Karina Scaramuzzi et. al)[10]

2.2 HBsAg

The hepatitis B surface antigen(HBsAg) envelops the hepatitis B virus, and detection of HBsAg in the body is used to diagnose Hepatitis B infection. HBsAg is also the primary component of hepatitis B vaccines as it causes the body to generate antibodies towards the virus.
HBsAg is a large protein consisting of more than 389 amino acids, and with a diameter of 22 nm[11]. Consequentially the protein is to big to fit inside the 10 nm mesopores of SBA-15. Interestingly, even though the protein is too large to be protected inside the mesopores, it has been shown SBA-15 can be used as adjuvant for HBsAg as oral vaccination, as the HBsAg protein is efficiently protected from the gastric acid.

3 Description of the Experimental Methods

3.1 Thermal analysis

Thermal properties of a material are measured during temperature changes. Thus, thermal analysis can reveal many different properties, such as phase transitions, water in confinement, decomposition etc. In this project thermogravimetric analysis combined with Fourier transformed infrared spectrometry(TGA-FTIR), and differential scanning calorimetry(DSC) are used to determine how HBsAg is confined within SBA-15.

3.1.1 Thermogravimetric analysis and Fourier transformed infrared spectrometry - TGA-FTIR

TGA is a method where the mass loss of a sample is measured during heating. The temperature at which mass loss occurs can be used to identify the composition of the sample,

or determine how confined a liquid, is inside the sample. The recorded mass loss can also be used to determine the amount of the evaporating material in the sample.

The molecules in the evaporating gases, in the TGA measurements, can be identified by attaching an infrared spectroscope, as follows.
Infrared spectroscopy sends electromagnetic radiation, in the infrared spectrum, through the evaporating gases. The photons can be absorbed by exciting the bonds in the molecules. The energy required for a bond to absorb a photon depends on the type of bonding and the mass of the atoms of the bond. Therefore the type of bonds and thereby the molecules in the gas can be identified by measuring the wavelength of the absorbed photons.
In Fourier transformed infrared spectrometry this is done by measuring the transmission of a wide spectrum in the infrared region. In the sensors the transmission signal of each wavelength is distinguished by a interferometer. The experimental signal is a interferogram which contains information of all used wavelengths. By Fourier transform of the interferogram an absorption spectrum is obtained. Often the wavenumber defined as $\frac{1}{\lambda}$ is used to distinguish the absorbtion instead of the wavelength λ.

3.1.2 Differential scanning calorimetry - DSC

DSC is a thermal analysis method that measures the difference in heat required to keep a sample and a reference at the same temperature while varying the temperature. The experimental signal is the sample's heat capacity. Peaks in the measured heat capacity during heating or cooling can be attributed to phase transitions in the material. The shape of the peak in the DSC signal can be used to determine the type of phase transition[12].

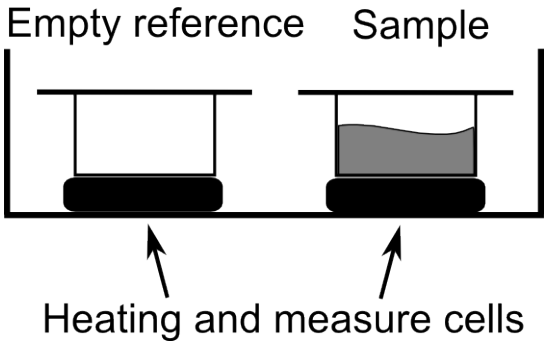

Figure 2: Sketch of a DSC setup. The empty reference crucible and the crucible containing the sample, are placed on the heating and measure cells, which measure the difference in energy required to keep the two samples at the same temperature during heating or cooling.

3.2 X-ray and Neutron imaging

In this project both neutron and X-ray imaging techniques were used. This section describes the basics of X-ray and neutron imaging as well as the basics of tomography.

3.2.1 Basic principles of X-ray imaging

In X-ray imaging, X-rays are sent through a sample and the transmission of the beam through different regions is recorded. Different elements attenuates the beam differently. High attenuating elements are then made visible by the decrease of the transmission.
X-rays are electromagnetic waves, and for a monochromatic wave propagating through a medium, the electric field can be described as.

$$E(\mathbf{r}) = E_0 e^{-in\mathbf{k}\cdot\mathbf{r}} \tag{1}$$

Where E_0 is the amplitude of the initial electric field, $\mathbf{k}$ is the wave vector $\mathbf{k} = \frac{2\pi}{\lambda}$, $\mathbf{r}$ is the spatial coordinate and n is the complex refractive index.

$$n = \kappa + i\beta. \tag{2}$$

By inserting (2) into (1) we get:

$$E(\mathbf{r}) = E_0 e^{-i(\kappa\mathbf{k}\cdot\mathbf{r})-\beta(\mathbf{k}\cdot\mathbf{r})} \tag{3}$$

So the real part of $\mathbf{Re}[n] = \kappa$ is related to the phase of the propagating wave and the imaginary part $i\beta$ is related to the amplitude of the wave as it propagates through the media.

If the wave propagates in the x direction the intensity averaged over time, of the electromagnetic field $I(x) = \frac{1}{2}\sqrt{\frac{\epsilon}{\mu_m}}|E(x)|^2$ can be written as.

$$I(x) = \frac{1}{2}\sqrt{\frac{\epsilon}{\mu_m}}E_0^2 e^{-\mu x} = I_0 e^{-\mu x}$$

Where ϵ is the electric permittivity, μ_m is the magnetic susceptibility of the media, $\mu \equiv 2\mathbf{k}\beta$ is the attenuation coefficient, with the unit $\frac{1}{cm}$, and I_0 is the initial intensity. So the higher μ the more the X-ray beam is attenuated by the material. The attenuation comes from interaction of the photons with the electron cloud of the attenuating element. The attenuation happens as absorption of photons through the photoelectric effect and scattering of the photons.
The likelihood of a photon being absorbed is determined by the absorption cross section which scales as $\frac{Z^4}{E^3}$, where Z is the atomic number and E is the energy of the X-rays. Scattering of the photons is dominated by Compton scattering in which the photons scatter of the electrons. Often it is better to use the mass attenuation coefficient $\left(\frac{\mu}{\rho}\right)$, where ρ is the density of the material. When performing X-ray imaging μ of a voxel can be measured, and if the mass attenuation coefficient of the material is known, the density of material in the voxel can be calculated as.

$$\rho_v = \mu_m \left(\frac{\mu}{\rho}\right)^{-1} \tag{4}$$

Where ρ_v is the density of material in the voxel, and μ_m is the measured attenuation coefficient.
The mass attenuation as a function of the photon energy for some different elements and materials is shown in fig. 3(a). It is seen that hydrogen attenuates much less than heavier elements, because of the absorption scaling as $\frac{Z^4}{E^3}$. This is why X-ray imaging is not very good at observing hydrogen and other light elements such as Lithium, but is good at detecting heavier elements.

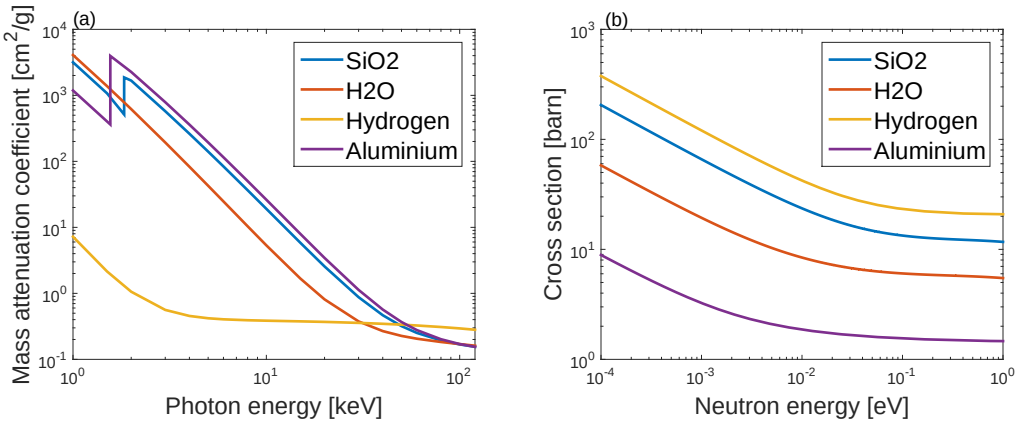

Figure 3: (a)X-ray mass attenuation coefficient for different element and compounds, data reproduced from National Institute of Standards and Technology[13]. (b)Total neutron cross sections for various elements as function of neutron energy, data reproduced from the National Nuclear Data Center[14].

3.2.2 Basic principles of neutron imaging

Neutron imaging similarly to X-ray imaging is a method which relies on attenuation. A beam of neutrons is guided towards the sample which attenuates the beam. While X-rays are attenuated by interaction with the the electron cloud the neutrons interact with atomic nuclei. This results in elements attenuating X-rays and neutron differently, so neutrons can be used to observe material that cannot be observed with X-ray and the other way around. An example of this is hydrogen which weakly interacts with X-ray, but attenuates neutrons strongly.

The attenuation of the neutron beam, makes the intensity decay exponentially just as for the X-ray.

$$I = I_0 e^{-\mu x}$$

The attenuation coefficient for neutrons μ can be written as.

$$\mu = \frac{\sigma_{total} \cdot \rho \cdot A}{m} \tag{5}$$

Where ρ is the density of the attenuating element, A is Avogadro's number, m is the atomic mass, and σ_{total} is the total cross section. The cross section is a number for how likely a neutron is to interact with the atomic nuclei. The cross section is defined as $\frac{\text{number of neutrons interacting pr. second}}{\text{neutron flux}}$ and has the unit cm^2, but is often expressed in the unit barn where 1 barn $= 10^{-24}\text{cm}^2$. The total cross section consist of the cross section for absorption and cross section for scattering as $\sigma_{total} = \sigma_{absorb} + \sigma_{Scatt}$. The cross section depends on the energy of the neutrons as seen in fig.3(b). In this project cold neutrons were used, which are neutrons with energy in the range $0.0 - 0.025eV$.

3.2.3 Computed tomography

In computed tomography 2D X-ray or neutron images are taken from various orientations of the sample is used to reconstruct its 3D map of the attenuation coefficient, $\mu(x, y, z)$. A method of doing this is to slightly rotate the sample in front of the source and detector, as seen in fig.4. Then make an image and rotate by the same amount again until the sample has rotated either a half revolution (180°) or a full revolution (360°). For a cone beam where the beam spot increases as it propagates, a full revolution scan provides the best results.

The spatial resolution of the images is determined by the detector screen specifications and the geometry of the set up. The detector plate is made with a grid of detection pixels, which each count the number of photons or neutrons. The emitted beam from the source is a cone beam where the spot size of the beam increases as the beam propagate as seen if fig.4. The increase of spot size leads to a magnification of the sample projection onto the detector screen. So the magnification of the sample gets higher when the detector is far away or the source is close to the sample. The magnification can be written as $M = \frac{SDD}{SOD}$ where the distances SOD and SDD are described in fig.4. The pixel size of reconstructed images can then be found as $PS_{im} = \frac{PS_{detector}}{M}$. Where PS_{im} is the image pixel size and $PS_{detector}$ is the pixel size of the detector. The disadvantage of moving the detector further away to gain high magnification, is that the beam spot increases and the intensity for each detector pixel decreases.

For neutron imaging the beam spot increases so rapidly that the detector in reality needs to be placed as close to the sample as possible to obtain a strong signal. To gain any magnification in this situation an artificial focal point, from which the beam spot increases, can be designed by a neutron guide after the source. The right neutron guide will place the artificial focal point very close to the sample.

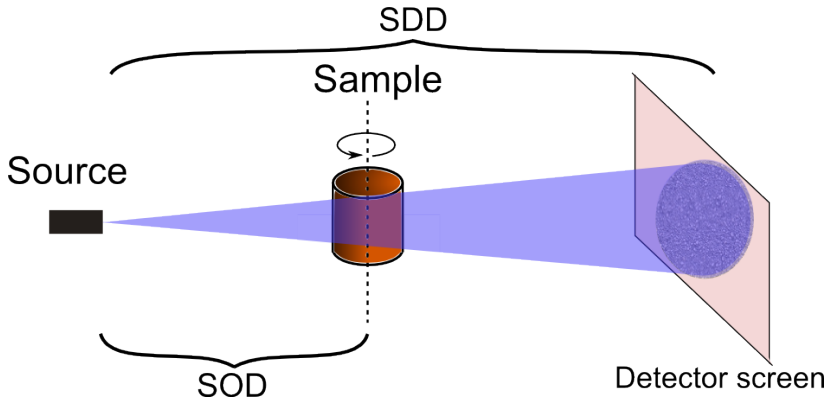

Figure 4: Drawing of a tomography set up, with the marked distances, source to object(SOD) and source to detector(SDD).

The data from the measurements is reconstructed by cutting the images in slices perpendicularity to the rotation axis, of the same height as the effective pixel size. Each of these slices is then reconstructed into a 2D grayscale image which represents a map of the attenuation coefficient $\mu(x, y)$ of the slice, called a tomogram. Each pixel in the tomogram represents a volume element of the sample, with the size of the efficient pixel size cubed. If the attenuating elements are well known, the density can be calculated from the measured attenuation coefficient with eq.(4) or eq.(5) for X-ray or neutrons, respectively.

For calculations of the density, beam hardening can be a cause of error. Beam hardening occurs if the source output is not monochromatic. As seen in fig.3(a) and fig.3(b), both X-rays and neutrons with low energy gets more attenuated than those with higher energies. So when the beam propagates through the sample the lower energies get attenuated and the average energy rises, and the beam gets hardened. This will especially occur if the outer parts of the sample is highly attenuating. This effect results in underestimated attenuation coefficients in the middle of the sample, compared to the initial wave spectrum.

4 Experimental details

In this section the analysed samples and the conducted experiments are described.

4.1 The samples

For HBsAg to be used as an vaccine within the SBA-15 structure, the HBsAg protein is diluted into a phosphate buffered solution(PBS), which is a aqueous salt solution, before being added to the SBA-15. The PBS molecules are small enough to possibly be confined within the mesopores in SBA-15.

In this project four different samples were used:

-Pure SBA-15 containing neither PBS or HBsAg, from now referred to as pure SBA-15.
-SBA-15 and PBS only, Contr..
-HBsAg and SBA-15 in ratio 1:40, with PBS, SBA-15 1:40.
-HBsAg and SBA-15 in ratio 1:2, with PBS, SBA-15 1:2.
So SBA-15 1:2 contains 20 times more vaccine than SBA-15 1:40.

All samples were provided by Márcia Fantini from the University of São Paulo, Brazil.

4.2 Thermal analysis

4.2.1 TGA-FTIR

For the TGA measurements a TG 209 F1 Libra® from Netzsch with an attached ALPHA FTIR spectrometer from Bruker, was used. The measurements were conducted on all four samples, with masses ranging $6-10$ mg pr. sample in an aluminium crucible. The samples were heated from 30°C to 1050°C at $10\frac{^{\circ}\mathrm{C}}{\mathrm{min}}$. The FTIR measurements were made in the wavenumber spectrum 500 to 4500 cm^{-1}.

4.2.2 DSC

DSC 214 Pulyma from Netsch was used to perform the DSC measurements. The measurements were performed by heating from 30°C to 500°C at $10\frac{^{\circ}\mathrm{C}}{\mathrm{min}}$. Measurements were made for all samples mounted in a pinned crucible. A set of measurements of SBA-15 and SBA-15 1:2 mounted in closed crucibles were also made.

4.3 Imaging

4.3.1 Neutron and X-ray imaging at Helmholtz Center Berlin

Neutron and X-ray imaging where performed at the Helmholtz Center in Berlin. The samples where mounted in cylinder aluminium sample holders with a diameter of 1 cm and height of 4 mm. Neutron images of all four samples were conducted in the CONRAD instrument. The neutrons are created in the research reactor BER II, and are slowed down in a water filter and feeded to the CONRAD instrument, which has a setup as fig.4, through the neutron guideline[15]. CONRAD has a detector with a pixel size of 50μm, and by the geometry of the setup a magnification of 7.84 was gained, thereby an effective pixel size of 6.37μm was achieved.
X-ray measurements at the Helmholtz Center were made in a setup as fig.4. The pixel size of the detector was 50μm and by the geometry of the setup a magnification of 7.84 resulting in a pixel size of the images of 6.37μm.
The software OctupusReconstructer was used to reconstruct the data to tomograms.

4.3.2 X-ray imaging at the Technical University of Denmark(DTU)

X-ray images were obtained from DTU using a Xradia VersaXRM-410, which has a set up as fig.4. The pixel size of the detector was 13μm. Measurements of, Contr., SBA-15 1:40 and SBA-15 1:2, were made with a geometrical magnification of 1.42 and a 4x magnification from an optical lens, resulting in a pixel size of 2.29μm.
A measurement was made of SBA-15 1:2 with a geometrical magnification of 1.32, and a 10x optical lens resulting in a pixel size of 0.98μm. The software XRMreconstructor was used to reconstruct the data to tomograms.

5 Results and discussion

5.1 TGA

The results of the TGA measurements are shown in fig.5.

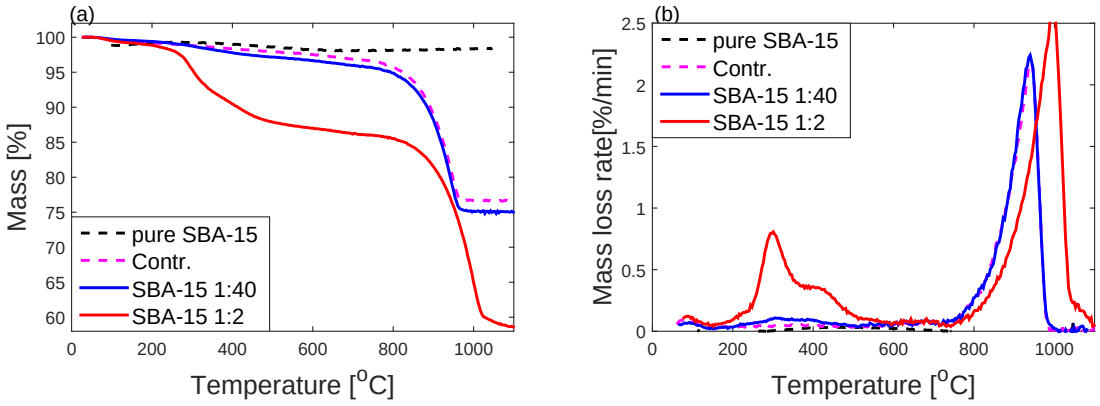

Figure 5: (a)TGA signal. (b)The first derivative of the measured TGA signal.

From fig.5 it can be observed that all samples have an initial mass loss between 20°C and 100°C. This can be attributed to the vaporization of water, absorbed by the samples from the air.
The pure SBA-15 shows no other mass loss during heating, therefore the mass loss for the Contr. sample which starts at 800°C comes from release of the PBS. As this is a very high temperature for the release of PBS, it suggests that PBS is strongly confined in the SBA-15 structure, possibly absorbed in or adsorbed on the surfaces of the 10 nm mesopores.
For the SBA-15 1:2 the same kind of mass loss is seen starting at 800°C, but another significant mass loss is observed at 300°C. For SBA-15 1:40 a mass loss can also be observed at 300°C although much smaller. The mass losses at 300°C must then be attributed to the vaccine, and shows that the HBsAg is confined within the SBA-15 structure but not as strongly as the PBS. This fits well with the HBsAg being too large to fit within the mesopores.
These observations lead to the following question: Is HBsAg being dehydrated from the

strongly confined PBS or is PBS+HBsAg leaving the SBA-15 structure at 300°C and thereby confined different than the strongly bound PBS.

5.2 FTIR

In fig.6 and fig.7 the absorption spectrum of Contr., SBA-15 1:40 and SBA-15 1:2 at 300°C and 880°C are shown respectively. The absorption signal from the experiment presents a low intensity, resulting in the instrument not being able to correct exactly for water and CO_2 in the experimental atmosphere. This resulted in a negative CO_2 peak for all samples, which have been removed from fig.6 and fig.7. Therefor all peaks observed in the region 1300cm^{-1} to 2000cm^{-1} can mostly be attributed to bad compensation of water in the atmosphere.
During the mass loss at 300°C absorption peaks are observed at 1750 cm^{-1}, 2120 cm^{-1}, 2190 cm^{-1} and 2820 cm^{-1} for SBA-15 1:2, see fig.6. The peak at 1750 cm^{-1} can be attributed to the stretching of C=O bonds, which are common in amino acids, the building blocks of the protein. The peaks at 2120 cm^{-1} and 2190 cm^{-1} are assigned to CO in the evaporating gas, and the peak at 2820 cm^{-1} can be attributed to C-H$_n$ bonds[16, 17]. So organic material which can only be from the HBsAg protein is evaporating from the SBA-15 structure. For SBA-15 1:40 neither the CO or C-H$_n$ peak are observed and eventual C=O peaks are indistinguishable from the water spectrum. This is attributed to the signal being too weak to be observed from the small amount of HBsAg in SBA-15 1:40. For Contr. no significant peak is observed as one would expect, as there is no mass loss at this temperature.

At 880°C in fig.7 the CO peaks are the only significant peaks in the spectrum for SBA-15 1:2. As the HBsAg is the only organic material in the sample, and these peaks are not present in Contr. is can be concluded that HBsAg is also present in evaporation from the SBA-15 structure in the mass loss at starting at 800°C. Thus we can conclude that two types of confinement of HBsAg within SBA-15 exists.

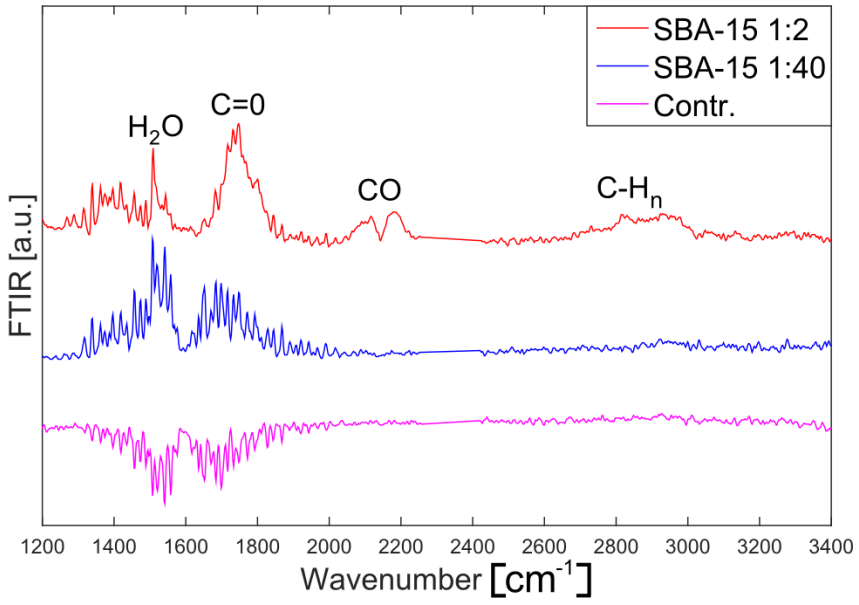

Figure 6: Absorption spectrum for Contr., SBA-15 1:40 and SBA-15 1:2 at 300°C related to the TGA measurements shown in fig.(5).

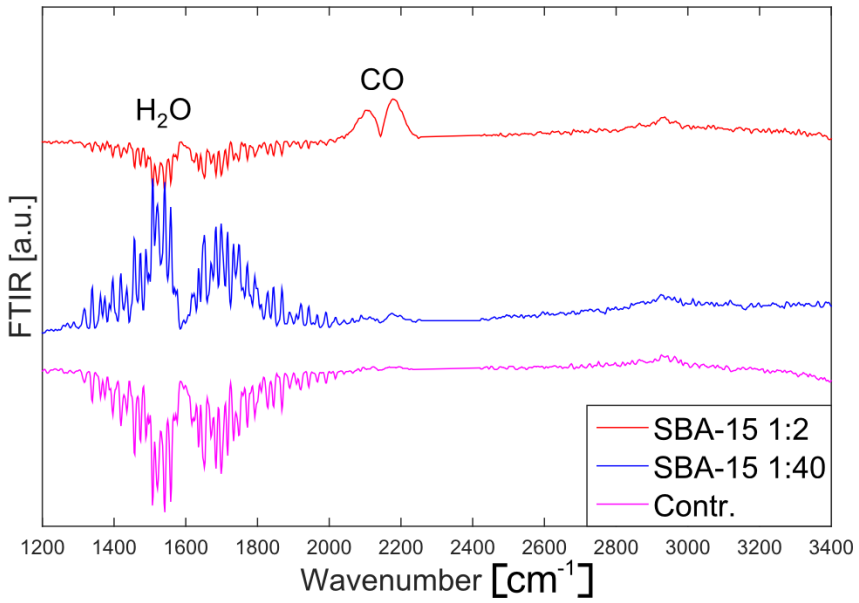

Figure 7: Absorption spectrum for Contr., SBA-15 1:40 and SBA-15 1:2 at 880°C related to the TGA measurements shown in fig.(5).

5.3 DSC

The results of the DSC measurements are seen in fig.8. The open crucible measurements in fig.8(a) shows the evaporation of water as observed in the TGA measurement. A peak for SBA-15 1:2 at 250°C, which is where the mass loss containing HBsAg was observed to start in the TGA measurements. For the closed crucible measurements fig.8(b) the water peak has disappeared, and two new sharp peaks are observed instead. This behaviour when measuring for both open and closed crucibles, correspond to the water being dehydrated from SBA-15 in the open crucible case, as reported by D.Giron[18]. The location and shape of the last peak in SBA-15 1:2 at 250°C marked by an arrow in fig.8, is unchanged, so this transition is not a dehydration of HBsAg from PBS. This supports the earlier point that the mass loss at 250°C observed in the TGA measurement are both due to the HBsAg and the PBS leaving the SBA-15 structure.

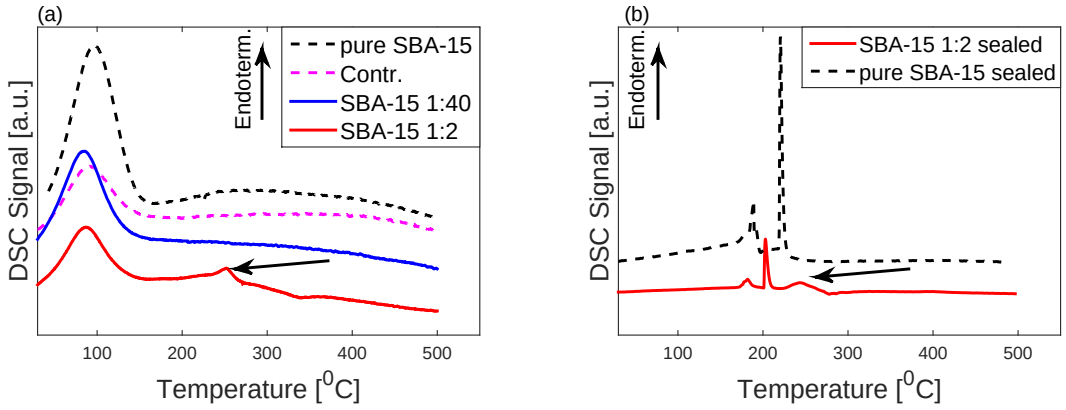

Figure 8: DSC signal. (a)For open crucibles. (b)Closed crucible. Arrows pointing at peak at 250°C with the same shape for both open and closed crucible, showing that HBsAg is not being dehydrated from PBS.

5.4 Neutron and X-ray imaging at Helmholtz Center Berlin

2D tomograms for each sample from neutron and X-ray imaging, from the Helmholtz Center, are shown in fig.9 and fig.12, respectively. The brighter the image the more the neutron or X-ray beam have been attenuated. The outer ring is the aluminium sample holder, and it is easily seen how different the aluminium attenuates the neutron and X-ray beam.

In the neutron images in fig.9(a) no contrast is observed for pure SBA-15. So the contrast observed in the other samples, must be due to the added PBS or HBsAg. In fig.9(b) the PBS, in the Contr. sample, shows up in small lumps, and also forms some characteristic long curved lines. The structures of such a curved line have been 3D reconstructed in fig.10 where it shows as a thin curved surface.

The SBA-15 1:40 in fig.9(c) shows lumps of contrast, which is generally larger than those observed in the Contr. sample. A very large branched structure with a length of

about 1.8mm is also present in the SBA-15 1:40. This structure has been 3D reconstructed in fig.11 where the branching is easily seen. This indicates that the HBsAg agglomerates in large structures. These structures must be built by HBsAg filling up macropores and then interconnecting the macropores in large branching structures. From this it is also seen that the agglomerated HBsAg is not distributed uniformly throughout the sample as a large amount is confined in a relatively small area of the sample. In fig.9(d) which contains 20 times more vaccine than SBA-15 1:40, a large amount of agglomerated HBsAg throughout the sample is seen.

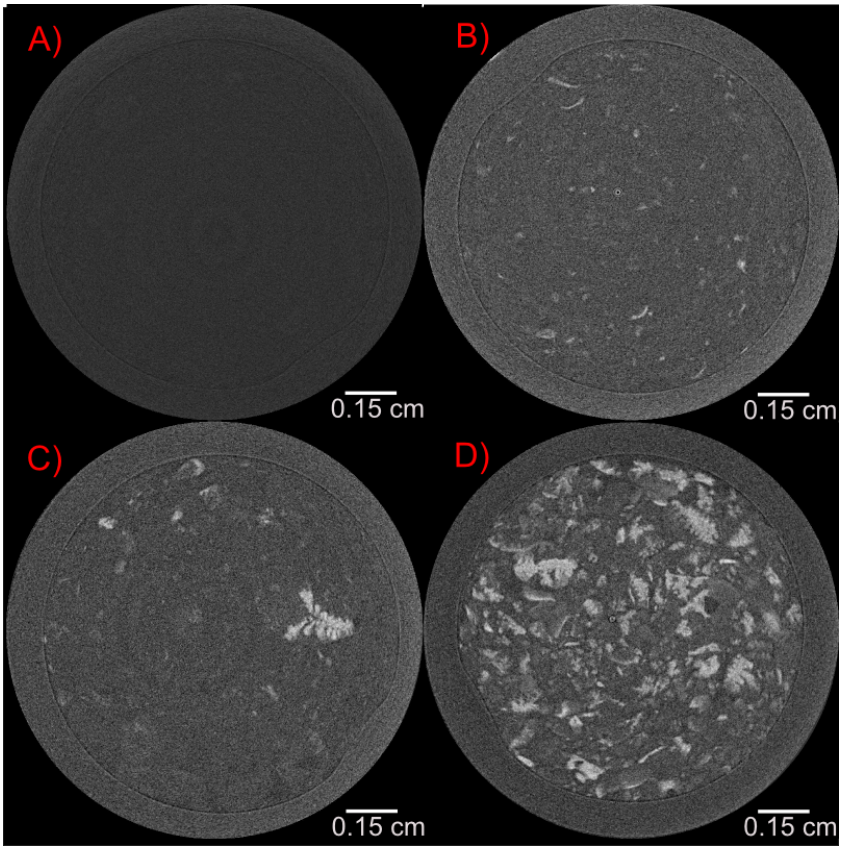

Figure 9: Neutron imagesobtained at the CONRAD instrument at Helmholtz Center Berlin, with a pixel size of 6.37μm. The diameter of the samples are 1 cm.(a)pure SBA-15 (b)Contr. (c)SBA-15 1:40 (d)SBA-15 1:2.

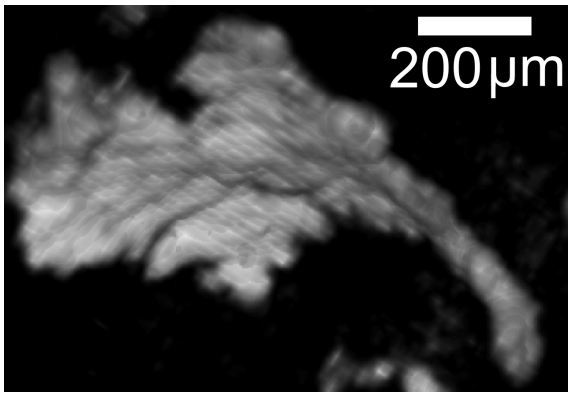

Figure 10: 3D reconstructed of a curved line PBS structure in Contr. sample from neutron data fig.9(b). The length of the structure is about 0.9 mm.

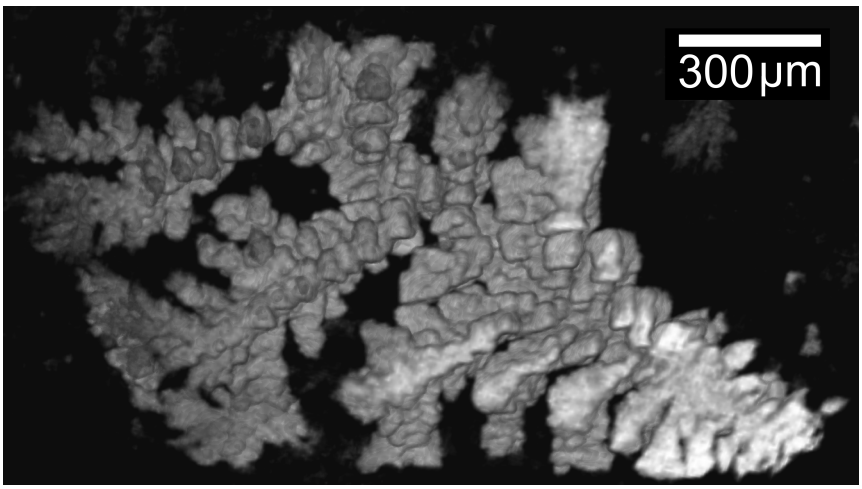

Figure 11: 3D reconstruction of the large agglomeration structure from SBA-15 1:40 observed in fig.9(c) with a length of 1.8 mm.

The X-ray images in fig.12 were obtained with the exact same samples as the neutron imaging, and are directly comparable. The same agglomeration are present in both images. The similarity of the structures can be calculated by first setting a threshold for how much the beam must be attenuated in a pixel to be considered a part of the agglomeration structure. Then by comparing the neutron and X-ray images of the large agglomerated structure observed in SBA-15 1:40, a similarity of $90\pm1\%$ is calculated, meaning that when an agglomeration pixel is observed in the neutron image 90% of the time the X-ray has a agglomerated pixel at the same spot. So the structures that are observed in the neutron and X-ray images are the same. However the element that attenuates the neutrons can not be the same as those that attenuate the X-ray. The neutron beam is mainly attenuated by the hydrogen in the HBsAg and PBS. The X-ray beam is, in contrast, attenuated by high densities of silica SiO_2. Consequently the agglomeration of HBsAg and PBS might

contract the silica rods in SBA-15, to generate high density of SiO_2. This might happen by PBS attaching to the mesopores of the rods around the macropores, and thereby gluing the rods together.

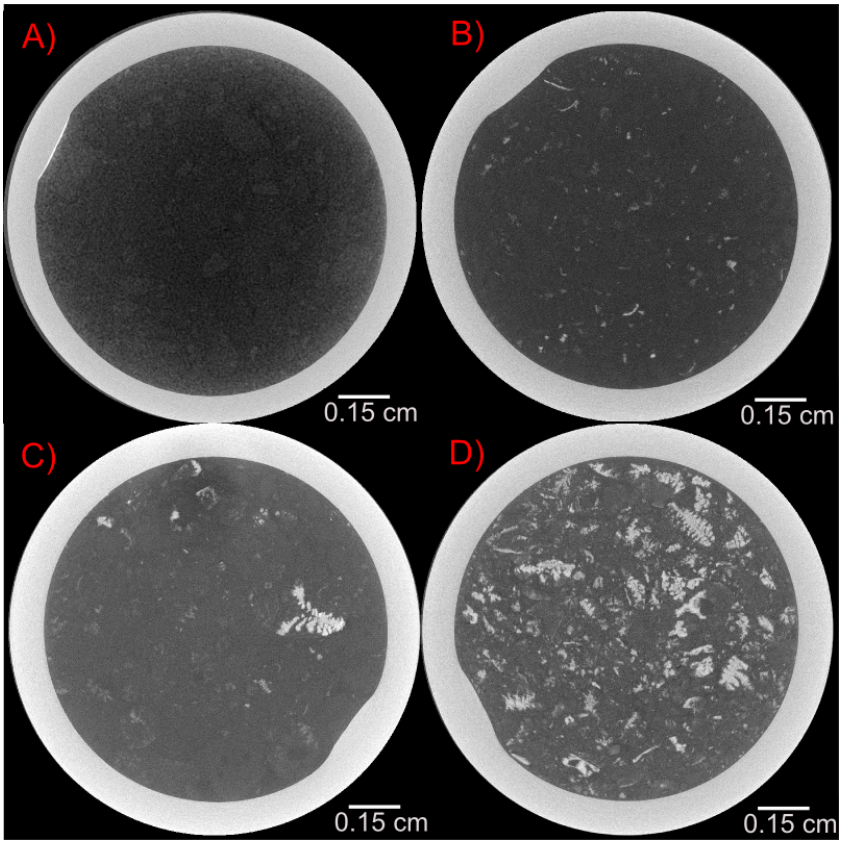

Figure 12: X-ray images obtained at the Helmholtz Center Berlin with a pixel size of 6.37. The diameter of the samples are 1 cm. (a)pure SBA-15(Contrast been enhanced considerably to see small inhomogeneities for pure SBA-15, which will be further discussed in section 5.5) (b)Contr. (c)SBA-15 1:40 (d)SBA-15 1:2.

The attenuation due to the hydrogen in the neutron measurements can be obtained as follows. The required density of SiO_2, to attenuate the X-rays as seen in fig.12 can be calculated using eq.(4) and how much this same density of SiO_2 attenuates the neutrons can then be calvulated using eq.5. Then the neutron attenuation coefficient for SiO_2 is subtracted from the total neutron attenuation coefficient and one gets the attenuation from hydrogen as:

$$\mu_H = \mu_{All} - \mu_{SiO_2} \tag{6}$$

Where μ_H is the attenuation caused by hydrogen in the neutron measurements, μ_{All} is the measured attenuation of the sample and μ_{SiO_2} is the total calculated attenuation from SiO_2. The data from the X-ray and neutron imaging was reconstructed into 16-bit data,

and scaled such that the attenuation coefficient range -1 to $10\frac{1}{cm}$ were linearly scaled in the integer range 0 to 65536. So from the images the attenuation coefficient of a pixel can be found as.

$$\mu = -1 + \frac{11}{65536} \cdot pixelvalue$$

The mean μ_{SiO_2} is calculated by the mean of the pixel values in the agglomerated structures. To calculate ρ_{SiO_2}, a tabulated $\left(\frac{\mu}{\rho}\right)$ is required which can be found knowing the photon energy. The effective photon energy can be found from the observed attenuation of the X-ray beam from the aluminium sample holder which has the density $\rho_{Al} = 2.70\frac{g}{cm^3}$.

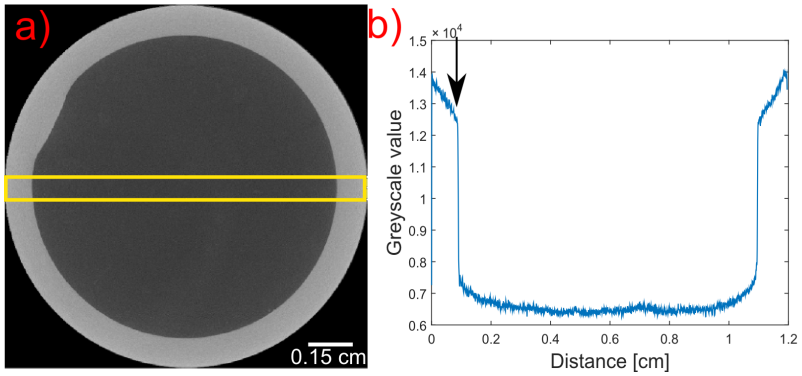

Figure 13: (a) The yellow box shows the area where the grayscale values have been averaged in y direction and plotted in (b) as function of x. (b)Plot of averaged grayscale values as function of x. The beam hardening is observed as the grayscale values of the aluminium sample holder decrease rapidly. The black arrow marks the area of the grayscale value used to calculate attenuation coefficient for aluminium.

The attenuation coefficient at the marked point in fig.13(b) is used to calculate the photon energy which propagates through the sample. This gives the mass attenuation coefficient $\left(\frac{\mu}{\rho}\right) = (0.39 \pm 0.02)\frac{\text{cm}^2}{\text{g}}$ which corresponds to a X-ray energy of (38.5 ± 0.6)keV[19]. For this energy the tabulated $\left(\frac{\mu}{\rho}\right)$ value for SiO_2 is $\left(\frac{\mu}{\rho}\right) = (0.506 \pm 0.02)\frac{\text{cm}^2}{\text{g}}$[13]. Now the mean μ_{SiO_2} and ρ_{SiO_2} in the four samples can be calculated. The results are shown in Table 1.

For the neutrons the effective energy or wavelength can be determined in the same way. In fig.14 it can be seen that the beam hardening effect of the neutrons is much less than for X-ray as the aluminium sample holder attenuates neutrons much less. The measured attenuation coefficient of the aluminium is $(0.13 \pm 0.01)\frac{1}{cm}$ and by (5) the cross section is found to be $\sigma_{Al} = (2.28 \pm 0.12)$ barn which corresponds to the neutrons having a wavelengths of (2.37 ± 0.15)A, which fits well with being cold neutrons[20]. For this wavelength the cross section of hydrogen is $\sigma_H = (108 \pm 4)$ barn. With eq.(6) and eq.(5)

the mean density and total mass of hydrogen in the agglomerations can be calculated. These results are seen in Table 1.

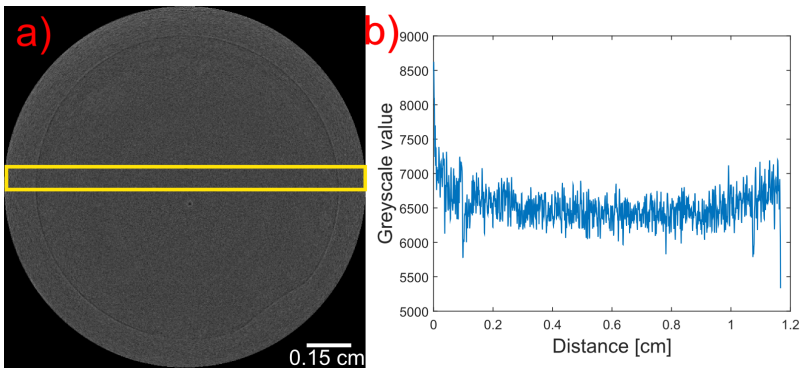

Figure 14: Beam hardening for Neutron.
(a) The yellow box shows the area where the grayscale values have been averaged in y direction and plotted in (b) as function of x. (b)Plot of averaged grayscale values as function of x. Beam hardening is observed to be weak compared to X-ray case.

Sample	$\mu_{\mathrm{SiO_2}}[\frac{1}{\mathrm{cm}}]$	$\rho_{\mathrm{SiO_2}}[\frac{g}{cm^3}]$	$\mu_{\mathrm{H}}[\frac{1}{\mathrm{cm}}]$	$\rho_{\mathrm{H}}[\frac{g}{cm^3}]$	$m_{\mathrm{H}}[g]$
Contr.	0.70±0.02	1.38±0.07	0.64±0.03	(9.9±0.4)x10^{-3}	(4.0±0.2)x10^{-6}
SBA-15 1:40	0.76±0.03	1.49±0.08	0.77±0.05	(11.9±0.6)x10^{-3}	(15.4±0.5)x10^{-6}
SBA-15 1:2	0.79±0.01	1.57±0.07	0.84±0.02	(13.0±0.3)x10^{-3}	(211±6)x10^{-6}

Table 1: The mean value of μ_{SiO_2} and ρ_{SiO_2} obtained from X-ray measurements, and the mean μ_H and ρ_H from the Neutron images, and the total hydrogen mass in the agglomeration structures of the samples.

From the results in Table 1, it can be seen that the hydrogen density in the agglomerating areas are higher for the samples containing HBsAg than the Contr. Thereby we can conclude that these agglomerations do in fact contain the protein which has many amino acids containing large amount of hydrogen atoms. It is also observed that the density of hydrogen and thereby HbsAg in the agglomerations is higher for the larger ratio of vaccine so the agglomeration of vaccine is tighter.
With the method used to obtain the results in Table 1, the amount of hydrogen in the large structure in the SBA-15 1:40, shown in fig.9(c), can be calculated. The amount of hydrogen in this agglomeration is (7.8 ± 0.7)x10^{-6}g and $(54 \pm 1)\%$ of all hydrogen atoms in this SBA-15 1:40 sample are agglomerated in this structure, which volume is only 0.7% of the entire sample. So the agglomerated vaccine is not uniformly distributed throughout SBA-15.

5.5 X-ray imaging at DTU

A tomogram for each of the X-ray measurements at DTU is shown in fig.15. In these X-ray images the curved PBS lines and HBsAg agglomerations are again seen, however a new type of structure is also observed. These are less attenuating regions that looks like flakes in the images. These regions can also be observed vaguely in the pure SBA-15 sample in fig. 12(a), and is due to inhomogeneity in the SBA-15 powder. These regions have lengths in the range $100\mu\text{m} - 1000\mu\text{m}$ so it can be attributed to grains or collections of grains in the SBA-15 powder. In the Contr. sample it is seen that the high SiO_2 contrast which occurs from PBS is on the surface of the grains or have not penetrated very far into the grains. So the curved surface created by the PBS, as seen in the 3D reconstruction in fig. 10, occurs as PBS coats the surface of the grains. This can be attributed to the PBS attaching to or filling the mesopores on the surface of the grains as already pointed out by the thermal analysis presented in 5.1. In the case of HBsAg+PBS the agglomerations take place inside the grains, in the macroporosities as can be seen in fig. 15(b)-(d).

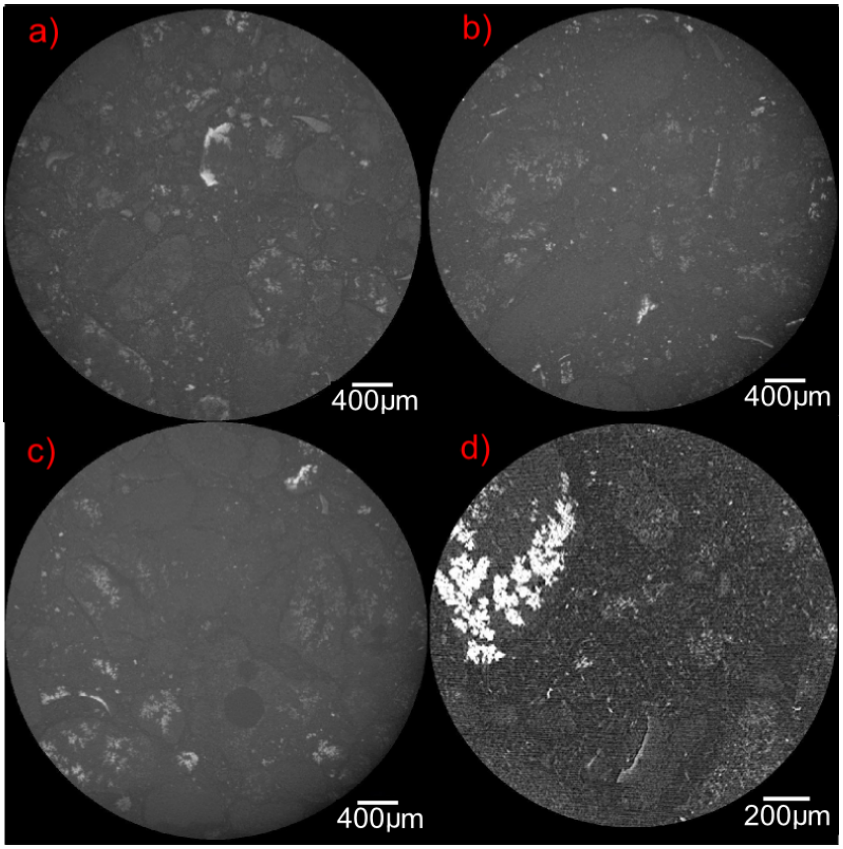

Figure 15: X-ray images made at DTU with a pixel size of 2.29 μm and sample diameter of 0.4 cm for (a-c), and a pixel size of 0.98 μm and sample diameter 0.16 cm for (d). (a)Contr. (b)SBA-15 1:40 (c)SBA-15 1:2 (d) SBA-15 1:2.

6 Conclusion and perspective

TGA measurements, fig.5, showed that pure PBS starts evaporating from the SBA-15 nano structure at 800°C and thereby is strongly confined in SBA-15, probably by being absorbed in the 10 nm mesopores. For the samples containing HBsAg, another mass loss was observed at 300°C.
From the FTIR measurements, shown in fig.6 and fig.7, it was concluded that HBsAg protein leaves SBA-15 at both 300°C and 800°C.
DSC measurements, in fig.8, showed that PBS was also evaporating with HBsAg at 300°C. So from these experiments it can be concluded that the HBsAg can be confined in two different ways in the SBA-15 structure.
In the neutron and X-ray experiments it was observed that pure PBS is coating the the surface of the grain structures in SBA-15, fig.15. This coating of the grain structure could occur by PBS being absorbed in the mesopores SBA-15. For the samples containing HBsAg it was observed, fig.9, that the protein agglomerates in large branching structures. Such a agglomeration structure was 3D visualized in fig.11. These agglomeration structures was observed inside the SBA-15 grain structures and are the results of HBsAg filling and interconnecting the macropores.
Density calculations from the neutron and X-ray experiments determined that the agglomerations glues together the SiO_2 in higher densities, and that the sample SBA-15 1:2 contain higher densities of hydrogen and thereby more HBsAg in the agglomerations than what was observed in SBA-15 1:40. These calculations also showed that for the sample containing the least amount of HBsAg, SBA-15 1:40, the protein in the agglomerations is not necessarily evenly distributed throughout SBA-15. The example of this was that $(50 \pm 1)\%$ of the observed HBsAg in the SBA-15 1:40 sample in fig.9(c) was agglomerated in one structure with a volume corresponding to 0.7% of the measured sample.
The HBsAg observed in the agglomerations can be attributed to the first mass loss in the TGA measurements. The second mass loss of HBsAg from the TGA measurements can be attributed to stronger confinement of HBsAg, possibly from the adsorption of the 22 nm HBsAg proteins on top of the mesopores openings. This could happen on the rods in the edges of the already filled macropores, or on the rods throughout the sample, which would also lead to more evenly distribution of the HBsAg protein throughout the sample.
These hypothesis can be studied in the future by the use of small angle neutron scattering. Other studies have showed positive immunological responses with ratios of HBsAg and SBA-15 in between 1:40 and 1:2, so it would be interesting to do imaging studies of these ratios also to see how much these agglomeration changes. SBA-15 is promising as adjuvant for other vaccines for which the proteins are smaller than the HBsAg protein, and thereby have the possibility to be absorbed inside the 10 nm pores of SBA-15, so it would also be interesting to perform neutron and X-ray imaging of these types of vaccines to whether these proteins also agglomerates as HBsAg.

References

[1] World Health Organization. http://www.who.int/mediacentre/factsheets/fs204/en/.

[2] Sundhed.dk. https://www.sundhed.dk/sundhedsfaglig/laegehaandbogen/mave-tarm/tilstande-og-sygdomme/lever/hepatitis-b/.

[3] Hepatitis B Foundation. http://www.hepb.org/hepb/statistics.htm.

[4] Nikolai Petrovsky and Julio César Aguilar. "*Vaccine adjuvants: current state and future trends*". In: Immunology and Cell Biology 82.5 (2004), pp. 488–496.

[5] Luciana V Carvalho et al. "*Immunological parameters related to the adjuvant effect of the ordered mesoporous silica SBA-15*". In: Vaccine 28.50 (2010), pp. 7829–7836.

[6] Valeria Ambrogi et al. "*Use of SBA-15 for furosemide oral delivery enhancement*". In: European Journal of Pharmaceutical Sciences 46.1 (2012), pp. 43–48.

[7] Lina Wang and Ross L Coppel. "*Oral vaccine delivery: can it protect against non-mucosal pathogens?*" In: Informa Healthcare London (2008).

[8] F Mariano-Neto et al. "*Physical properties of ordered mesoporous SBA-15 silica as immunological adjuvant*". In: Journal of Physics D: Applied Physics 47.42 (2014), p. 425402.

[9] Michal Kruk et al. "*Characterization of the porous structure of SBA-15*". In: Chemistry of materials 12.7 (2000), pp. 1961–1968.

[10] Karina Scaramuzzi et al. "*Nanostructured SBA-15 silica as an adjuvant in immunizations with hepatitis B vaccine*". In: Einstein 9.4 (2011).

[11] Ira Berkower et al. "*Hepatitis B virus surface antigen assembly function persists when entire transmembrane domains 1 and 3 are replaced by a heterologous transmembrane sequence*". In: Journal of Virology 85.5 (2011), pp. 2439–2448.

[12] Phase Transitions and Differential Scanning Calorimetry. http://www.dartmouth.edu/~pchem/75/pdfs/DSC.pdf.

[13] National Institute for Standards and Technology. http://physics.nist.gov/PhysRefData/XrayMassCoef/tab3.html.

[14] National Nuclear Data Center. http://www.nndc.bnl.gov/sigma/index.jsp?as=16&lib=endfb7.0&nsub=10.

[15] Berlin CONRAD Instrument Helmholtz Center. https://www.helmholtz-berlin.de/forschung/oe/em/werkstoffe/methoden/n-tomo_en.html.

[16] Antonio Marcilla et al. "*Characterization of microalgal species through TGA/FTIR analysis: Application to nannochloropsis sp.*" In: Thermochimica Acta 484.1 (2009), pp. 41–47.

[17] Table of IR Absorptions University of Colorado. http://orgchem.colorado.edu/Spectroscopy/specttutor/irchart.pdf.

[18] D Giron. "*Investigations of polymorphism and pseudo-polymorphism in pharmaceuticals by combined thermoanalytical techniques*". In: Journal of Thermal Analysis and Calorimetry 64.1 (2001), pp. 37–60.

[19] X-Ray attenuation & absorption calculator. http://web-docs.gsi.de/~stoe_exp/web_programs/x_ray_absorption/index.php.

[20] ILL neutron calculator. http://www.ill.eu/?id=13156.

[21] Hanne Nøkleby. "*Neurological adverse events of immunization: experience with an aluminum adjuvanted meningococcal B outer membrane vesicle vaccine*". In: Informa Healthcare London (2007).

[22] Heermann KH et al. "*Large surface proteins of hepatitis B virus containing the pre-s sequence.*" In: Journal of Virology 52.2 (1984), pp. 396–402.

[23] Dace Skrastina et al. "*Silica Nanoparticles as the Adjuvant for the Immunisation of Mice Using Hepatitis B Core Virus-Like Particles*". In: PloS one 9.12 (2014), e114006.